Stability Analysis for a Borehole to be Drilled into the Tohoku Fault Zone, Japan

Stephanie Nale

Advisor: Emily Brodsky
Earth and Planetary Sciences Department
University of California, Santa Cruz
March 22, 2012

Table of Contents

List of Illustrations……...……..iii

Abstract……....v

Introduction…….……1

Farfield Stress Models……..……...……6

Stress Concentration Around a Borehole…….9

Strength of Fault Zone Materials……...12

Predictions of Borehole Stability…….……..……13

Results……...…….15

Andersonian Reverse Fault……15

Shallow-dip Fault at Failure……..….21

Andersonian Normal Fault…….24

Discussion……..……..……..….26

Conclusion.....31

References Cited……...…….33

List of Illustrations

Table 1: Assumed values used in calculations for farfield stress and borehole perimeter stress calculations.....……...10

Table 2: Results of stability analyses for the planned borehole by farfield stress regime, drill depth and rock strength.....31

Figure 1. Geographic location of the great Tohoku-Oki March 11, 2011 earthquake.....2

Figure 2. Seismic reflection data from before and after the March 11, 2011 Tohoku-Oki earthquake.....3

Figure 3. Proposed Sites JFAST-3 (primary) and JFAST-4 (alternate) seismic line and cross-line.....5

Figure 4. Cross-sectional diagrams of orientations of the three principle stresses, σ_1, σ_2 and σ_3, within three farfield stress models.....7

Figure 5. Horizontal cross section of a vertical borehole and stresses exerted on the perimeter of the borehole.....11

Figure 6. Propogation of breakouts in stable and unstable wells.....14

Figure 7. Breakout width as a function of the intermediate principle stress, σ_2 for the Andersonian reverse fault farfield stress regime at 900 m sediment depth.....16

Figure 8. Mohr circles for each value of σ_2 between σ_3 and σ_1 at the azimuth of S_{hmin} (90°, 270°) and S_{Hmax} (0°, 180°) for the borehole at 900 m sediment depth.....18

Figure 9. Breakout width as a function of the intermediate principle stress, σ_2 for the Andersonian reverse fault farfield stress regime at 800 m sediment depth.....19

Figure 10. Mohr circles for each value of σ_2 between σ_3 and σ_1 at the azimuth of S_{hmin} (90°, 270°) and S_{Hmax} (0°, 180°) for the borehole at 800 m sediment depth.....20

Figure 11. Breakout width as a function of the intermediate principle stress, σ_2, for the shallow-dip reverse fault at failure stress regime at 900 m sediment depth.....22

Figure 12. Breakout width as a function of the intermediate principle stress, σ_2, for the shallow-dip reverse fault at failure stress regime at 800 m sediment depth.....23

Figure 13. Breakout width as a function of the intermediate principle stress, σ_2, for the Andersonian normal fault farfield stress regime at 900 m sediment depth.....24

Figure 14. Breakout width as a function of the intermediate principle stress, σ_2, for the Andersonian normal fault farfield stress regime at 800 m sediment depth.....25

Figure 15. Possible contingency sites.....30

Abstract

To study mechanisms that produce great subduction zone earthquakes such as the March 11, 2011 Tohoku-Oki earthquake, the Integrated Ocean Drilling Program (IODP) expedition 343 will engage in rapid response drilling into the recently ruptured fault. This expedition is based on the *Japan Trench Fast Earthquake Drilling Project (JFAST)* proposal 787, and is scheduled aboard the D/V *Chikyu* from April 1, 2012 through May 24, 2012. Prior to drilling, models are utilized to predict borehole stability under the intense pressure and stress conditions at the proposed drilling depth. In this study, the stresses acting within the proposed borehole were calculated to assess failure conditions for three possible farfield stress regimes: an Andersonian reverse fault, a critically stressed shallowly dipping (5°) reverse fault, and an Andersonian normal fault. The intermediate principle stress in each farfield stress model is allowed to vary from the value of the minimum to the maximum principle stress. The stress concentration around the circumference of the borehole is determined by the principle stresses acting within the horizontal plane of the vertical borehole. Failure by borehole wall breakouts are expected in this horizontal plane, as determined by the value of the intermediate principle stress and the rock strength of the borehole wall. To achieve a greater range in our stability analysis, the coefficient of friction and cohesion of the local rock is varied according to reasonably high and low values for an accretionary prism. To test the sensitivity of the stress concentrations to depth, stability analyses are also examined at two possible drill depths. This study shows that failure of the borehole depends strongly on the farfield stress state and cohesion, and stability decreases with depth. Both catastrophic collapse and successful completion are possible for realistic scenarios.

Introduction

Rapid response drilling of recently ruptured faults can provide important information about faulting and rupture processes of large earthquakes that cannot be directly obtained by other means. Quickly following a large seismic event, drilling operations can acquire measurements of temperature, stress and geologic data to study dynamic friction within the fault, strength, healing, faulting-related fluid flow, stress changes, and physical and chemical properties of a fault (Brodsky, *et. al.*, 2009). The great Tohoku-Oki earthquake (M_w 9.0) of March 11, 2011 is unique in both its large magnitude and that the fault ruptured updip to the surface of the trench, with the largest slip ever recorded in an earthquake, approximately 50 m (Mori, et al., 2011). The location of the Tohoku-Oki earthquake epicenter is shown in Figure 1.

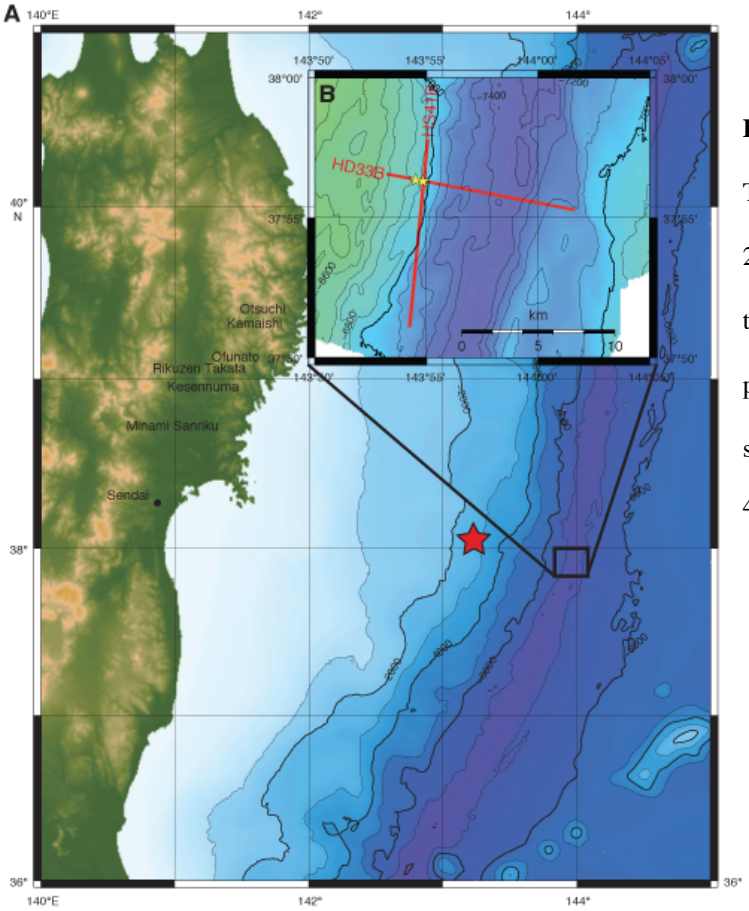

Figure 1. A. Large-scale map showing Tohoku region and epicenter of 11 March 2011 Tohoku earthquake (red star) along with the survey lines and IODP Expedition 343 proposed drill site (in box). **B.** Close-up map, showing proposed Sites JFAST-3 and JFAST-4. From Mori, *et. al.*, 2012, p. 22.

The depth, magnitude, large slip and rupture to trench of the Tohoku-Oki earthquake were unexpected based on previous studies (Mori, *et al.,* 2011). Drilling into the recently ruptured fault zone will provide data (i.e. fault zone physical properties, material samples, and temperature measurements as a proxy for stress released during slip), which can be utilized to better understand friction and faulting processes of large earthquakes (Mori, *et al.,* 2011). Seismic reflection data from before and after the event show that at about 7 km ocean depth, the fault would be intersected by a drill hole at approximately 800 m below the sea floor (Figure 2) (Mori, *et al*., 2012). There is great

potential for a large amount of information to be learned of faulting and earthquake mechanisms in subduction zone thrust faults from this planned drilling operation.

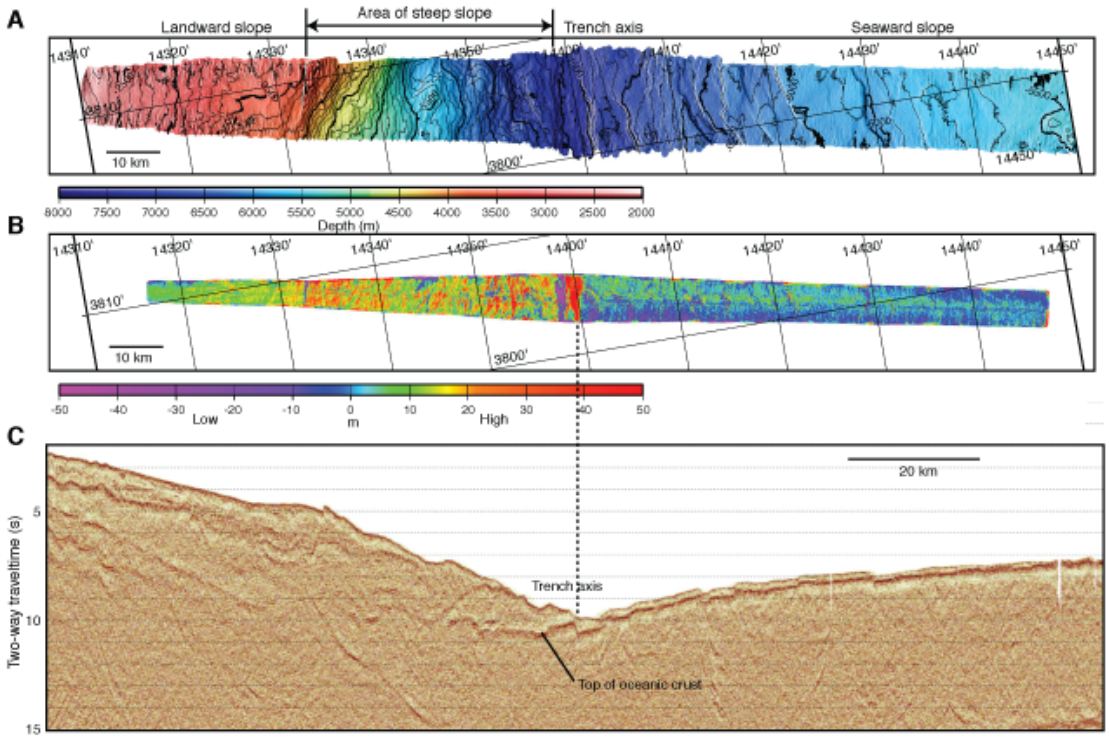

Figure 2. Coseismic displacement of the 2011 Tohoku earthquake extended all the way to the trench axis (Fujiwara et al., 2011). **A.** Bathymetric data along Line TH03. **B.** Difference between the bathymetric data acquired before (1999) and after (2011) the earthquake. **C.** Time-migrated multichannel seismic (MCS) section along Line TH03. Comparing B and C suggests that coseismic fault slip reached to the trench axis along the top of the basaltic layer (or an interface slightly above it) because the top of the basaltic layer and an interface slightly above it are the only visible interfaces in the MCS section. From Mori, *et. al.*, 2012, p. 23.

The Integrated Ocean Drilling Program (IODP) Expedition 343 will operate based on Proposal 787, titled *Japan Trench Fast Earthquake Drilling Project (JFAST)*, to

collect the data necessary for study of the mechanisms behind the unusual rupture of the Tohoku-Oki earthquake (Mori *et al.*, 2012). In order to meet the scientific objectives, the cased hole needs to be in place by January 2013 for the time-dependent initial studies as well as future observations and monitoring (Mori, *et al*., 2011). JFAST is scheduled for the D/V *Chikyu* from April 1, 2012 through May 24, 2012, a total of fifty-four days for the entire operation, including transit.

Two locations have been identified for drilling into the toe of the frontal prism of the megathrust, at the top of the oceanic basement (Figure 3). The primary site, JFAST-3, is located at 6910 m of ocean water depth and approximately 900 m into the sea floor (approximately 800 m to the target fault). The alternate site, JFAST-4 is located at 6830 m of water depth, and approximately 900 m below the sea floor, with the target fault at approximately 880 m sediment depth (Mori, *et. al.*, 2012).

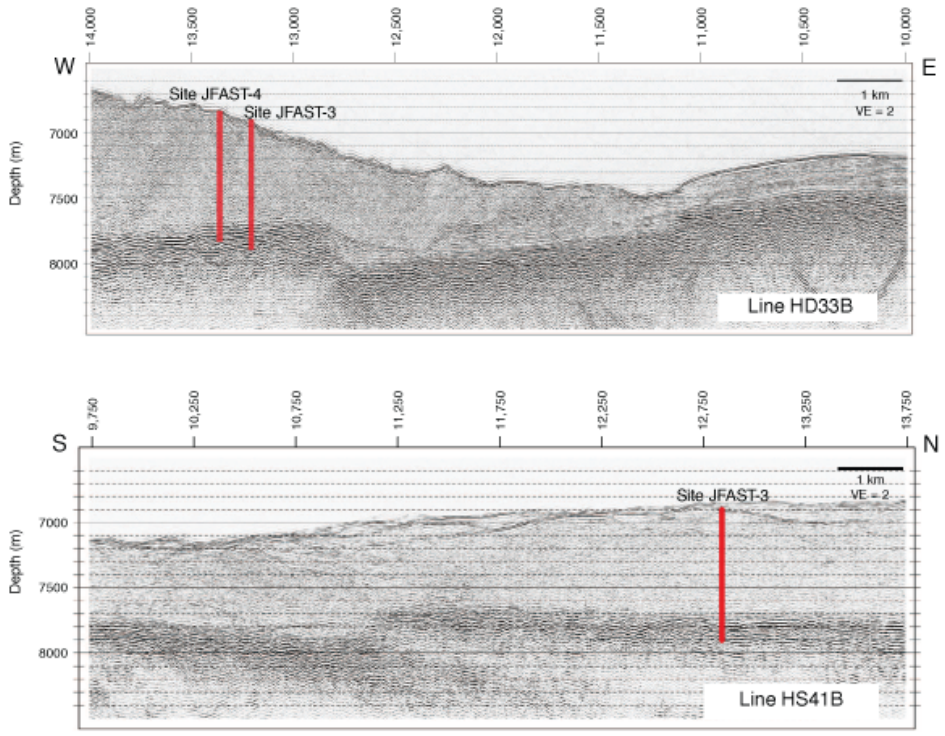

Figure 3. Proposed Sites JFAST-3 (primary) and JFAST-4 (alternate) seismic line and cross-line. From Mori, *et. al.,* 2012, p. 26.

Two holes will be drilled at the selected site. Hole A will include logging while drilling and measurement while drilling tools as well as a temporary pressure/temperature observatory that will be installed after casing of the hole. Cores will be collected from Hole B at approximately 300-400 m intervals, followed by casing and installation of another pressure/temperature observatory that is expected to last approximately 5 years (Mori, *et. al.*, 2012).

The rotary coring of a single borehole could take up to three weeks, during which time the borehole has the potential for catastrophic failure before casings can be put in place (Mori, *et al*., 2012). At present, only one hole has been successfully drilled at approximately the ocean depth of the planned JFAST sites. In May of 1978, the drilling

vessel *Glomar Challenger* successfully drilled 15.5 m into ocean sediment at Hole 461A, under 7034 m of ocean depth (Hussong, *et. al*., 1981). While the overburden pressure from the ocean at this site was comparable to, and even greater than, the overburden pressure from ocean water expected at the JFAST drill site, the comparatively shallow depth of the borehole into the sea floor indicates that Hole 461A is not a good prediction of success for JFAST.

To determine the feasibility of a borehole to be drilled into the Tohoku fault for research purposes, calculations must be completed to model the stresses acting on the borehole in the pressure conditions at the drilling depth, up to 7.9 km below sea level. This study will determine if the borehole will fail under assumed stress regimes, and aid in engineering design of the planned borehole.

Farfield Stress Models

According to E. M. Anderson's classification scheme, the orientation of the three effective principal stresses, σ_1, σ_2 and σ_3 (decreasing in magnitude) varies according to the farfield stress regime acting on the system (Anderson, 1951). In reverse faulting regimes, σ_1, σ_2 and σ_3 are the maximum horizontal stress, S_{Hmax}, minimum horizontal stress, S_{hmin}, and the vertical stress resulting from overburden pressure, S_v, respectively. Within normal faulting regimes, the principle stresses correspond to S_v, S_{Hmax}, and S_{hmin}.

The effective stresses acting within the stress regime are calculated from the real stresses, S_1, S_2 and S_3 by the equation:

$$\sigma_m = S_m - P_p \qquad \textbf{(1)}$$

where P_p is pore pressure

The current farfield stress regime of the Tohoku fault zone following the great Tohoku-Oki earthquake is unknown, and will be examined from data collected by the JFAST operation. In order to determine potential stability of the planned borehole, we need to first assume appropriate farfield stress models to predict borehole stress concentrations. For these experiments, three end members were considered based on potential far-field stress conditions following the large rupture (Figure 4).

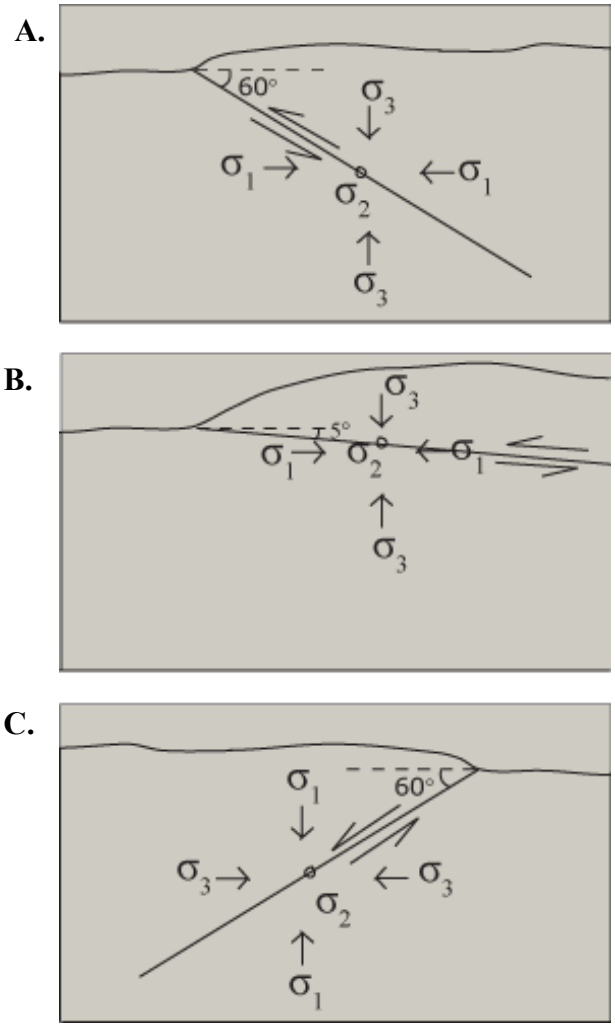

Figure 4. Cross-sectional diagrams of orientations of the three principle stresses, σ_1, σ_2 and σ_3, within three farfield stress models. **A.** The orientations of the principal stresses in an Andersonian reverse fault. **B**. The orientation of the principle stresses in a shallowly dipping reserve fault. **C.** The orientation of the three principal stresses in an Andersonian normal fault.

The first end member is modeled by the Andersonian definition for an optimally dipping reverse faulting regime

$$\frac{\sigma_1}{\sigma_3} = \frac{S_{Hmax} - P_p}{S_v - P_p} \leq [(\mu_i{}^2 + 1)^{1/2} + \mu_i]^2 \quad \textbf{(2)}$$

using the calculated real stresses, S_{Hmax} and S_v, the pore pressure, P_p, and the fault coefficient of friction, $\mu_i = 0.4$.

The optimal angle of the fault is 60°, using the fault coefficient of friction, μ_i in the equation

$$\theta_{opt} = 0.5\tan^{-1}(1/\mu_i) \quad \textbf{(3)}$$

The orientation of the Andersonian reverse fault and corresponding principle stress orientations are shown in Figure 4 A.

The second end member entailed using the calculation for shear stress, on a critically stressed fault dipping at 5° from horizontal based on the coefficient of friction and normal stress, σ_n.

$$\tau = \mu_i\sigma_n \quad \textbf{(4)}$$

where: $\tau = 0.5(\sigma_1 - \sigma_3)\sin(2\theta_{fault})$ **(5)**

and $\sigma_n = -0.5(\sigma_1 - \sigma_3)\cos(2\theta_{fault}) + 0.5(\sigma_1 + \sigma_3)$ **(6)**

and where θ_{fault} is the angle between the fault normal and σ_1:

$\theta_{fault} = 5°$

As shown in Figure 4 B, the orientation of the shallowly dipping reverse fault at failure is different (smaller angle) from the Andersonian reverse fault but the corresponding principle stresses are still in the same orientation.

The third end member examines an Andersonian normal faulting regime in which case the Tohoku fault zone would have evolved into an extensional farfield stress state after the March 11, 2011 event (Ide, *et. al.*, 2011).

$$\frac{\sigma_1}{\sigma_3} = \frac{S_v - P_p}{S_{hmin} - P_p} \leq [(\mu_i{}^2 + 1)^{1/2} + \mu_i]^2 \qquad \textbf{(7)}$$

The Andersonian normal fault is shown in Figure 4 C, and differs from the previous two farfield stress models by both the relative movement along the fault and the orientation of the principle stresses. The optimal angle of the normal fault is 60°, using the same fault coefficient of friction, ($\mu_i = 0.4$) from equation 3.

In all cases presented, the pore pressure, P_p, is hydrostatic,

$$P_p = \rho_{SW} g(d_{SF} + d_B) \qquad \textbf{(8)}$$

where ρ_{SW} is the density of sea water, g is the acceleration of gravity, d_{SF} is the depth to the sea floor and d_B is the depth of the borehole below the sea floor

The local borehole coefficient of friction, μ, is constrained below (See "Strength of Fault Zone Materials").

Stress Concentration Around a Borehole

For each farfield stress regime, we can predict the stresses acting on the perimeter of a borehole using the Kirsch equations (Zoback, 2010, p.174):

$$\sigma_{\theta\theta} = S_{hmin} + S_{Hmax} - 2(S_{Hmax} - S_{hmin})\cos(2\theta) - 2P_p - \Delta P \qquad \textbf{(9)}$$

where θ is the angle around the circumference of the borehole from the azimuth of S_{Hmax}

and $\Delta P = P_{mud} - P_p$ **(10)**

$$\sigma_{rr} = \Delta P \qquad \textbf{(11)}$$

$$\sigma_{zz} = S_v - 2\upsilon(S_{Hmax} - S_{hmin})\cos(2\theta) - P_p \quad \textbf{(12)}$$

where υ is Poisson's ratio

The Kirsch equations are typically used to calculate the *in situ* stress conditions after drilling by analyses of the width of stress-induced compressive failures (breakouts) produced on a borehole (Zoback, 2010). This study utilizes these equations to work backward from assumed *in situ* stress conditions (from the farfield stress regime models described above) to predict width of breakouts expected around the circumference of the boreholes to be drilled for JFAST.

Calculations for the hoop (circumferential) stress, $\sigma_{\theta\theta}$ (equation 9), radial stress, σ_{rr} (equation 11), and stress acting parallel to the borehole axis, σ_{zz} (equation 12), were produced in Matlab and based on assumed values for the Tohoku fault zone, i.e. internal coefficient of friction, cohesion, pore pressure, fault dip, rock density, and depth (Table 1).

Table 1: Assumed values used in calculations for farfield stress and borehole perimeter stress concentrations.

Depth to sea floor	d_{SW}	7000 m
Depth of borehole below sea floor	d_B	900 m
Depth to target fault below sea floor	d_F	800 m
Density of rock	ρ_R	2000 g/cm^2
Density of sea water	ρ_{SW}	1025 g/cm^2
Acceleration of gravity	g	9.81 m/s^2
Fault coefficient of friction	μ_i	0.4
Pore pressure (hydrostatic)	P_p	78 MPa
Circulating mud weight	P_{mud}	78 MPa
Poisson's ratio	υ	0.3
Dip angle for Tohoku fault (shallowly dipping fault)	θ_{fault}	5°
Rock cohesion	S_0	10 MPa – 15 MPa
Local borehole coefficient of friction	μ	0.2 – 0.6

The orientation of the stresses around the circumference of the borehole is shown in Figure 5.

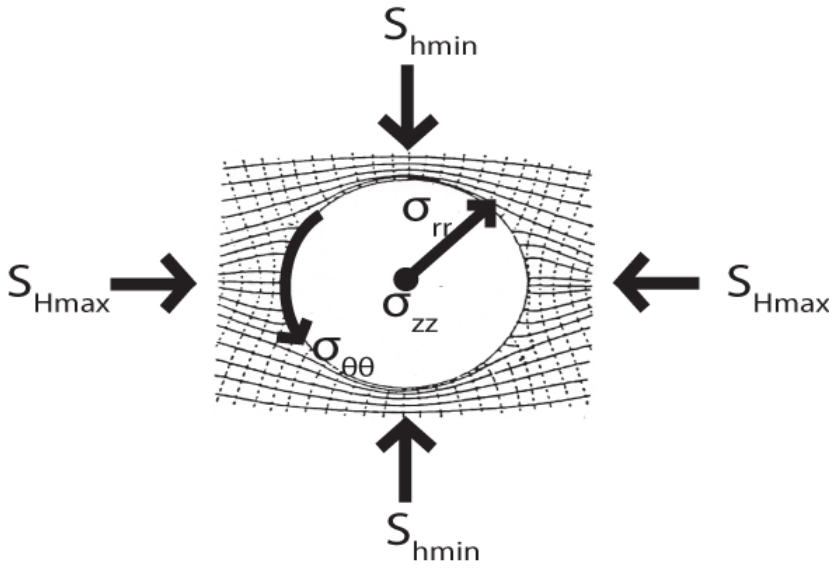

Figure 5. Horizontal cross section of a vertical borehole and stresses exerted on the perimeter of the borehole. The highest compressive stress occurs at the azimuth of S_{hmin}, while the least compressive stress occurs at the azimuth of S_{Hmax}. Modified from Zoback, 2010, p.169.

At present, it is not certain what density of mud will be used during drilling, so the change in pressure, ΔP, and therefore the radial stress, will be equal to zero ($\sigma_{rr} = 0$ MPa) in all cases considered in this study. Further discussion of the advantages and cautions concerning the potential of circulating mud during drilling will be presented below (See "Discussion").

The intermediate principle stress, σ_2, cannot be independently constrained in the preceding calculations for farfield stress models, but is necessary to calculate the stresses concentrating around the circumference of the borehole. The value of σ_2 must be between

the values of the maximum and minimum principle stresses ($\sigma_3 \leq \sigma_2 \leq \sigma_1$). In these calculations, σ_2, is defined as an array that varies between σ_3 and σ_1. For each model, a range of hoop stress values was calculated using the σ_2 array to study the stresses and resulting stability expectations in the system. The minimum horizontal stress, S_{hmin}, was then isolated from σ_2 to be used in the calculations for $\sigma_{\theta\theta}$ (equation 9).

Strength of Fault Zone Materials

For each farfield stress model considered, we must account for cohesive strength, S_0, and the coefficient of friction of the rock into which the borehole is drilled, μ, in addition to the hoop and radial stresses to describe stability of the borehole from the failure condition:

$$\tau_B > \tau_{fail} \quad \textbf{(13)}$$

$$\text{with: } \tau_{fail} = S_0 + \mu\sigma_{n_B} \quad \textbf{(14)}$$

where S_0 is the cohesion of the rock.

In the borehole:

$$\tau_B = 0.5(\sigma_{\theta\theta} - \sigma_{rr})\sin(2\phi) \quad \textbf{(15)}$$

$$\text{and} \quad \sigma_{n_B} = -0.5(\sigma_{\theta\theta} - \sigma_{rr})\cos(2\phi) + 0.5(\sigma_{\theta\theta} + \sigma_{rr}) \quad \textbf{(16)}$$

where ϕ is the angle around the circumference of the borehole from the azimuth of S_{Hmax}

To obtain a wider range of borehole stability predictions, both of these rock strength properties are examined at high and low values (Table 1).

The fault coefficient of friction, μ_i, is assumed to be a constant 0.4 for each model, whereas the local borehole coefficient of friction, μ, ranges from a lower value (μ

= 0.2) as measured in laboratory friction tests on quartz, illite shale, and smectite clay, common components of accretionary prisms (Marone and Saffer 2007) to $\mu = 0.6$ for harder rocks. Cohesion, S_0, is assumed to be between 10 MPa and 15 MPa, in accordance with work done by Marone and Saffer (2007). Disparities in the cohesive rock strength would be important to determining borehole stability in cases where the stresses are very near the failure condition. Such variations in cohesion could arise from chemical diversity and clay composition of the rock material (Marone and Saffer, 2007) as well as the extent of carbonate cementation of the rock within the fault zone (Moore, Rowe, and Meneghini, 2007).

Predictions of Borehole Stability

Calculations of the exerted stress and failure condition will determine the width of breakouts around the borehole wall circumference, which is a measure of how likely the borehole is to collapse in on itself. Because the stresses acting on the borehole wall vary with azimuth, stability of the borehole depends on the angular width and orientation of stresses around its perimeter (Zoback, 2010). Any point around the borehole where the shear stress (τ_B) acting on the system is greater than the shear stress at failure (τ_{fail}) will experience failure at that azimuth. The width of borehole wall where $\tau_B > \tau_{fail}$ is the width of failure of the rock. This failure around the circumference of the borehole wall will result in breakouts. Because of the compressive stress concentration around the borehole, breakouts will occur 180° apart, at the azimuth of S_{hmin} (Figure 5) (Zoback, 2010). The width of expected breakouts determines the likelihood of the proposed borehole to fail. Breakout widths exceeding 90° (180° total) are unstable and are expected to fail

completely (Zoback, 2010). Figure 6 A and B portray the propagation of breakouts in a stable and an unstable well, respectively.

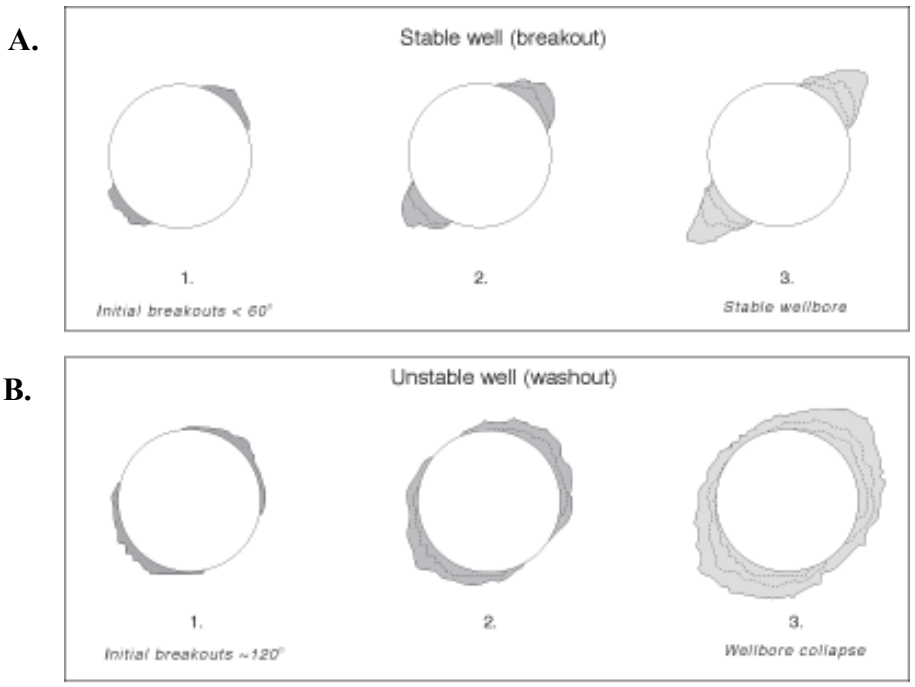

Figure 6. A. Narrow breakouts (< 60°) will deepen but not widen, resulting in a stable borehole. **B.** Wide breakouts (~120° shown) will continue to widen and result in borehole collapse. From Zoback, 2010, p. 304.

For all three farfield stress models, plots were produced for each value of σ_2, as described above, so that evolution of stability or failure of the borehole can be seen as the value of the intermediate stress increases within each potential stress regime. These graphs were reproduced for four cases, comparing each combination of μ and S_0, to test the effects of variations in rock strength and cohesion within the fault zone. To examine sensitivity of borehole stability to depth, tests were run at both 800 m depth below the sea

floor (the depth to the target fault in JFAST-3), and 900 m below sea floor (the total depth of the planned borehole).

Results

Calculations of borehole stress concentrations show a range of failure conditions for the proposed borehole, depending on the farfield stress regime, intermediate stress, drill depth, and rock strength properties.

Andersonian Reverse Fault

In the case of the Andersonian reverse farfield stress regime, failure of the borehole depends heavily on the values of the coefficient of friction, cohesion, and intermediate principle stress, as well as the depth of the borehole. Predictions range from a stable well to complete failure. Figure 7 A displays how the breakout width (W_B) varies for four different cases, depending on σ_2, μ and S_0 at 900 m depth below the sea floor. This figure (7 B-D) also shows the breakout width (W_B) at σ_3, $\overline{\sigma}_2$ and σ_1 (respectively) on a horizontal cross-section of the vertical borehole for case 1 ($\mu = 0.2$ and $S_0 = 10$ MPa). These polar plots of the failure around the borehole circumference show the greater compressive stress at the azimuth of S_{hmin}, and the least amount of compressive stress at the azimuth of S_{Hmax}.

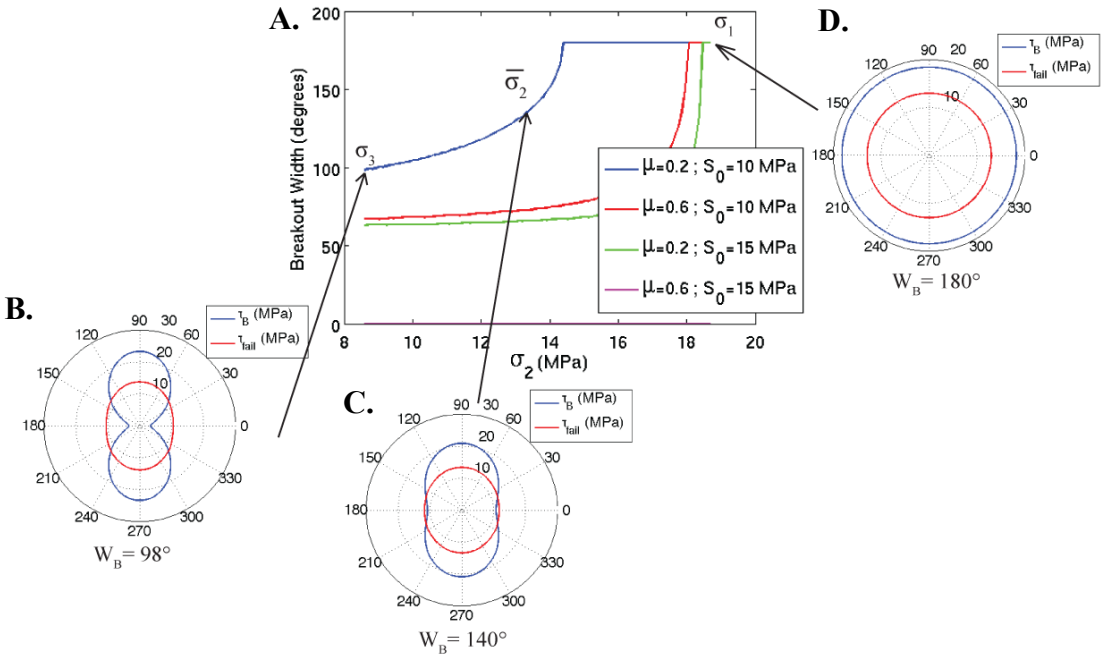

Figure 7. A. Breakout width as a function of the intermediate principle stress, σ_2, for the Andersonian reverse fault farfield stress regime at 900 m sediment depth. Four cases are considered, by combining reasonably high and low values of the coefficient of friction, μ, and the cohesion, S_0, of the rock. Polar plots of the shear stress acting around the circumference of the borehole are shown for case 1 (μ = 0.2 and S_0 = 10 MPa) of the Andersonian reverse fault stress regime at: **B.** $\sigma_2 = \sigma_3$, **C.** $\sigma_2 = \bar{\sigma}_2$, and **D.** $\sigma_2 = \sigma_1$. Where the failure condition is reached ($\tau_B > \tau_{fail}$), the borehole will experience breakouts at that azimuth. The azimuth of S_{hmin} is 90° and 270°, whereas the azimuth of S_{Hmax} is at 0° and 180°.

The four different cases considered within this farfield stress model do not follow the same trend of borehole breakout as a function of the intermediate principle stress, σ_2. For case 1, where μ = 0.2 and S_0 = 10 MPa, the borehole is in failure and the width of breakouts increases from approximately 90° to 180° as σ_2 approaches σ_1. An increase in

either μ or S_0 will result in a situation where the width of boreholes increases from just greater than 60° to complete failure of the borehole with an increase in σ_2. For the strongest rock, case 4, (where $\mu = 0.6$ and $S_0 = 15$ MPa), the borehole will be stable within the entire range of σ_2. Cases 2 ($\mu = 0.6$ and $S_0 = 10$ MPa) and 3 ($\mu = 0.2$, $S_0 = 15$ MPa) are both stable at $\sigma_2 = \sigma_3$, but breakout width increases rapidly when the intermediate stress approaches maximum value.

The evolution of breakout width as a function of the intermediate stress seen in Figure 7, particularly for cases 2 and 3, is further examined by producing Mohr circles at a specific azimuth around the borehole (Figure 8 A-D). From the azimuth of S_{hmin}, the greatest compressive stress, the Mohr circles are large initially and decrease in size as the value of σ_2 increases (approaching a more stable condition). From the azimuth of the least compressive stress, S_{Hmax}, the Mohr circles start out small and increase in as σ_2 approaches σ_3 (approaching a less stable condition). Wherever a Mohr circle exceeds the shear stress at failure, τ_{fail}, the failure condition is reached ($\tau_B > \tau_{fail}$) and the borehole wall is in failure at that azimuth and for that value of σ_2. The intermediate Mohr circle, towards which the Mohr circles at the azimuths of S_{hmin} and S_{Hmax} converge, describes the stability of the borehole where $\sigma_2 = \sigma_1$.

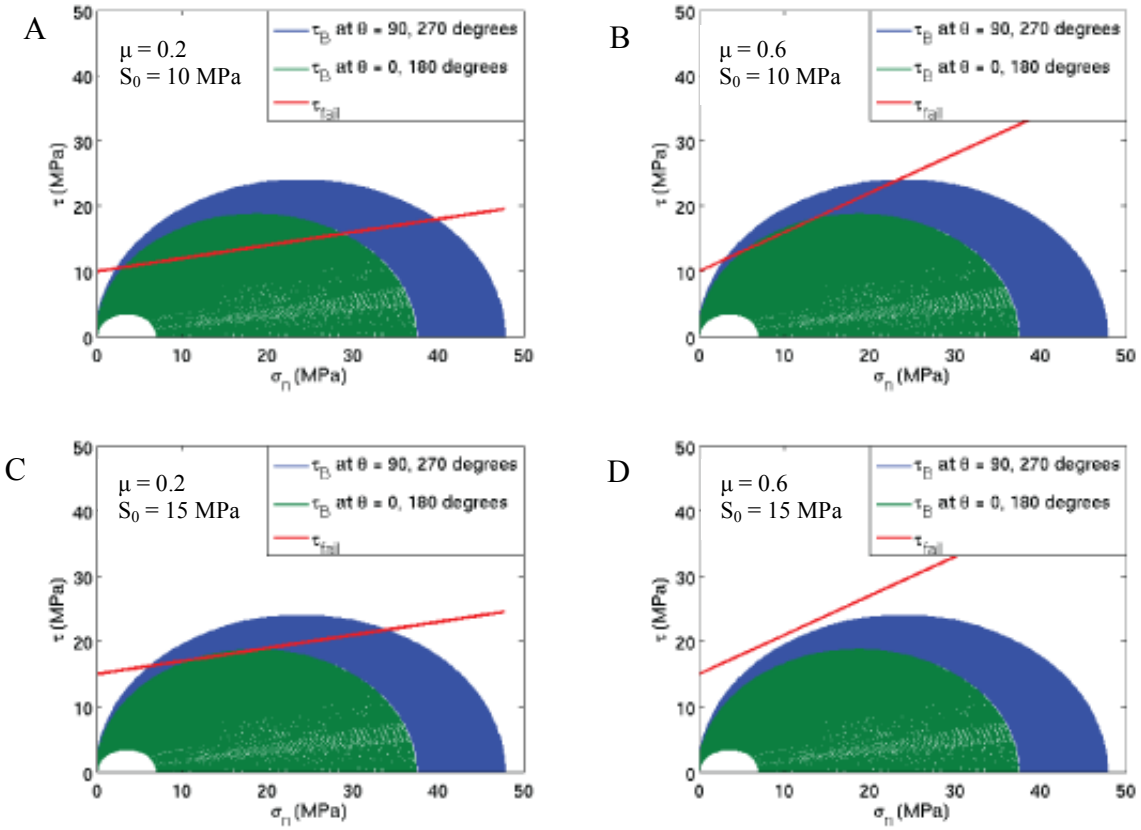

Figure 8. Mohr circles for each value of σ_2 between σ_3 and σ_1 at the azimuth of S_{hmin} (90°, 270°) and S_{Hmax} (0°, 180°) for the borehole at 900 m depth below sea floor. Mohr circles converge upon an intermediate stability condition from each azimuth, depending on the strength of the borehole wall. **A.** Case 1, where $\mu = 0.2$ and $S_0 = 10$ MPa. **B.** Case 2, where $\mu = 0.6$ and $S_0 = 10$ MPa. **C.** Case 3, where $\mu = 0.2$ and $S_0 = 15$ MPa. **D.** Case 4, where $\mu = 0.6$ and $S_0 = 15$ MPa.

At the depth of the target fault, 800 m sediment depth, the borehole can experience a range of stability scenarios, similar to that expected at 900 m depth below the sea floor, though magnitudes and failure potential are decreased (Figure 9 A-D).

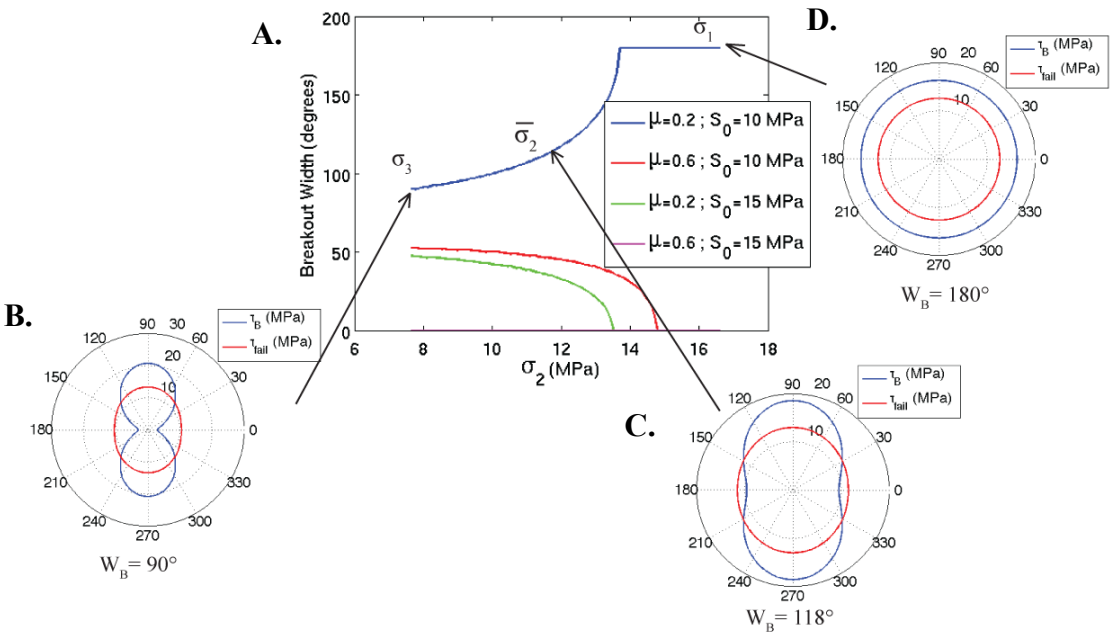

Figure 9. A. Breakout width as a function of the intermediate principle stress, σ_2, for the Andersonian reverse fault farfield stress regime at 800 m sediment depth. Four cases are considered, by combining reasonably high and low values of the coefficient of friction, μ, and the cohesion, S_0, of the rock. Polar plots of the shear stress acting around the circumference of the borehole are shown for case 1 (μ = 0.2 and S_0 = 10 MPa) of the Andersonian reverse fault stress regime at: **B.** $\sigma_2 = \sigma_3$, **C.** $\sigma_2 = \bar{\sigma}_2$, and **D.** $\sigma_2 = \sigma_1$. Where the failure condition is reached ($\tau_B > \tau_{fail}$), the borehole will experience breakouts at that azimuth. The azimuth of S_{hmin} is 90° and 270°, whereas the azimuth of S_{Hmax} is at 0° and 180°.

Overall, the borehole at 800 m depth below the sea floor is under less stress than at 900 m depth. For case 1, the borehole is in failure regardless of the value of the intermediate stress. Increasing either rock strength variables, however, produces a different evolution of borehole failure with intermediate stress change. In cases 2 and 3, the width of expected breakouts are large initially (close to 50°), but not failing, then

decrease with intermediate stress. Mohr circles at the azimuth of least (S_{Hmax}) and greatest (S_{hmin}) compressive stress show how the stability evolves from an unstable to stable condition in the borehole at the depth of the target fault (Figure 10). Because the magnitudes of stresses in the borehole are smaller at the reduced depth, the Mohr circles are smaller initially than at 900 m, and evolve toward a more stable borehole in cases 2 and 3. Case 4 is the strongest of the rock conditions studied, and is stable for the entire range of σ_2.

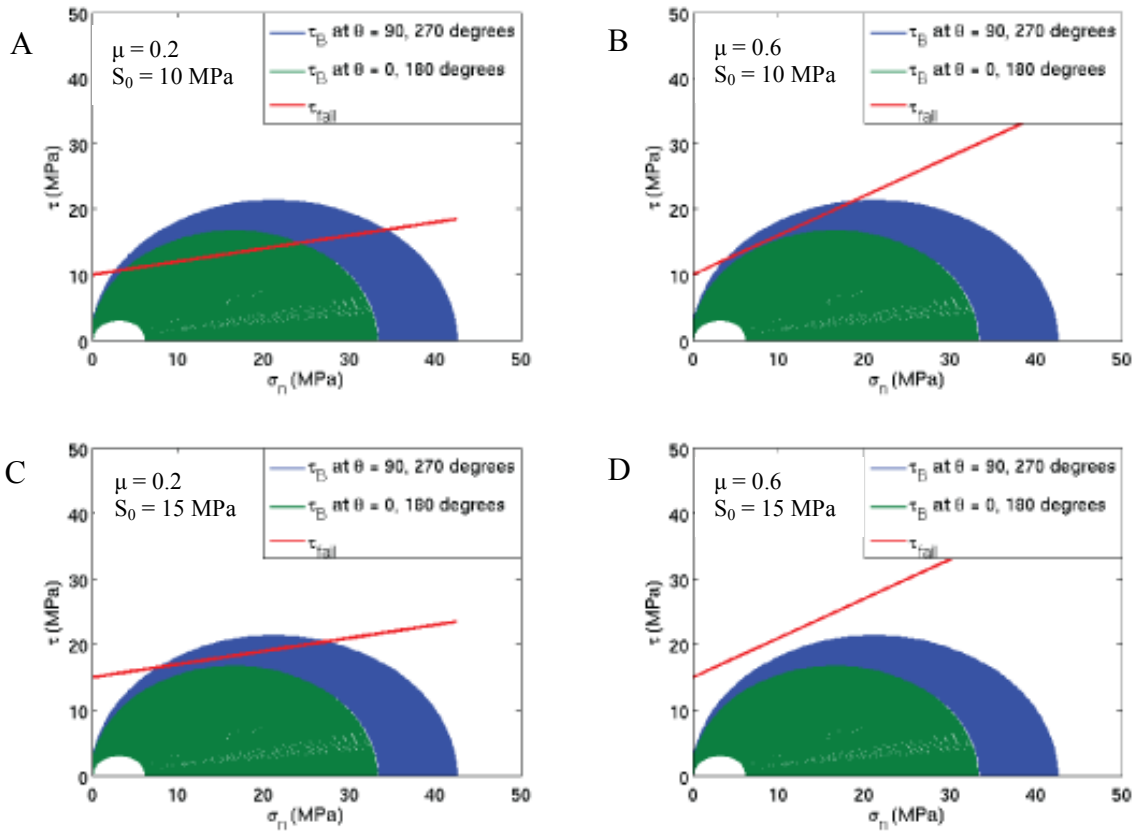

Figure 10. Mohr circles for each value of σ_2 between σ_3 and σ_1 at the azimuth of S_{hmin} (90°, 270°) and S_{Hmax} (0°, 180°) for the borehole at 800 m depth below sea floor. Mohr circles converge upon an intermediate

stability condition from each azimuth, depending on the strength of the borehole wall. **A.** Case 1, where $\mu = 0.2$ and $S_0 = 10$ MPa. **B.** Case 2, where $\mu = 0.6$ and $S_0 = 10$ MPa. **C.** Case 3, where $\mu = 0.2$ and $S_0 = 15$ MPa. **D.** Case 4, where $\mu = 0.6$ and $S_0 = 15$ MPa.

Shallow-dip Fault at Failure

The borehole at 900 m sediment depth within the stress regime of a shallowly dipping fault at failure is expected to fail completely at all cohesion and coefficient of friction combinations, and through the entire range of the intermediate stress, as seen in Figure 11 A. The total breakout widths increase from values greater than 90° to 180°, so that breakouts are occurring around the entire circumference of the borehole. Figure 11 B-D shows breakout width (W_B) at σ_3, $\overline{\sigma}_2$ and σ_1 (respectively) on a horizontal cross-section of the vertical borehole for case 1, where $\mu = 0.2$ and $S_0 = 10$ MPa, as an example.

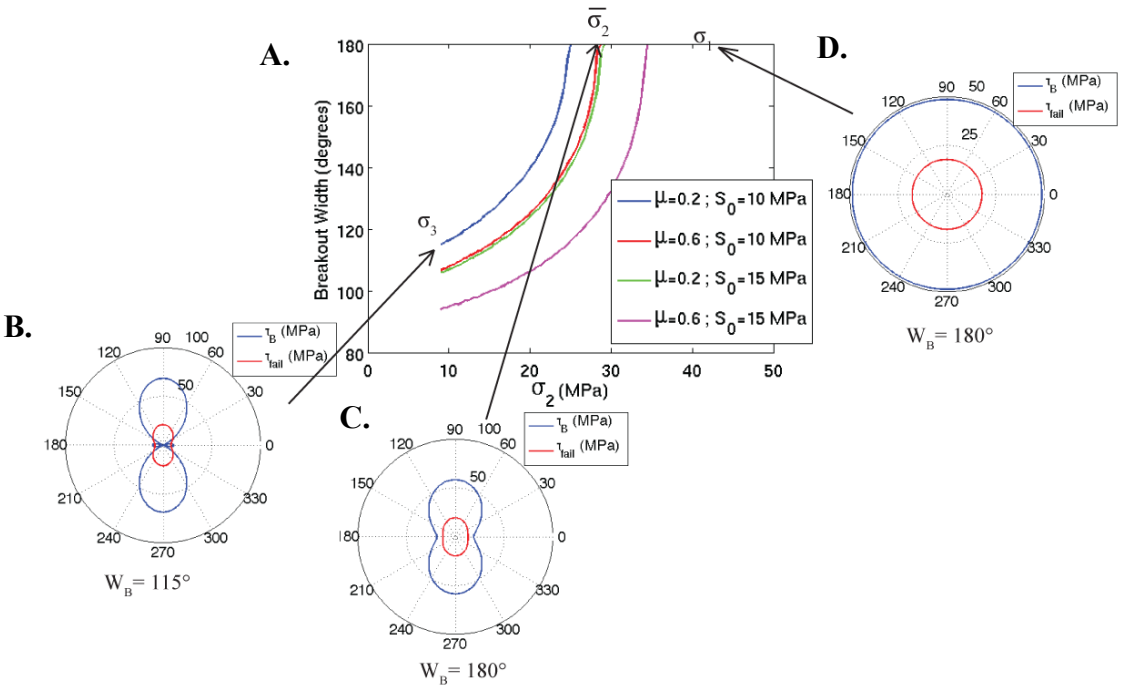

Figure 11. A Breakout width as a function of the intermediate principle stress, σ_2, for the shallow-dip reverse fault at failure stress regime at 900 m sediment depth. Four cases are considered, by combining reasonably high and low values of the coefficient of friction, μ, and the cohesion, S_0, of the rock. Polar plots of the shear stress acting around the circumference of the borehole are shown for case 1 (μ = 0.2 and S_0 = 10 MPa) of shallow-dip fault at failure stress regime at: **B.** $\sigma_2 = \sigma_3$, **C.** $\sigma_2 = \bar{\sigma}_2$, and **D.** $\sigma_2 = \sigma_1$. Where the failure condition is reached ($\tau_B > \tau_{fail}$), the borehole will experience breakouts at that azimuth. The azimuth of S_{hmin} is 90° and 270°, whereas the azimuth of S_{Hmax} is at 0° and 180°.

The borehole is still expected to be in complete failure at 800 m sediment depth, as seen in Figure 12 A-D. While the magnitude of exerted stresses, as well as the initial

width of resulting breakouts, is slightly lower at this shallower depth, the borehole is still expected to fail catastrophically.

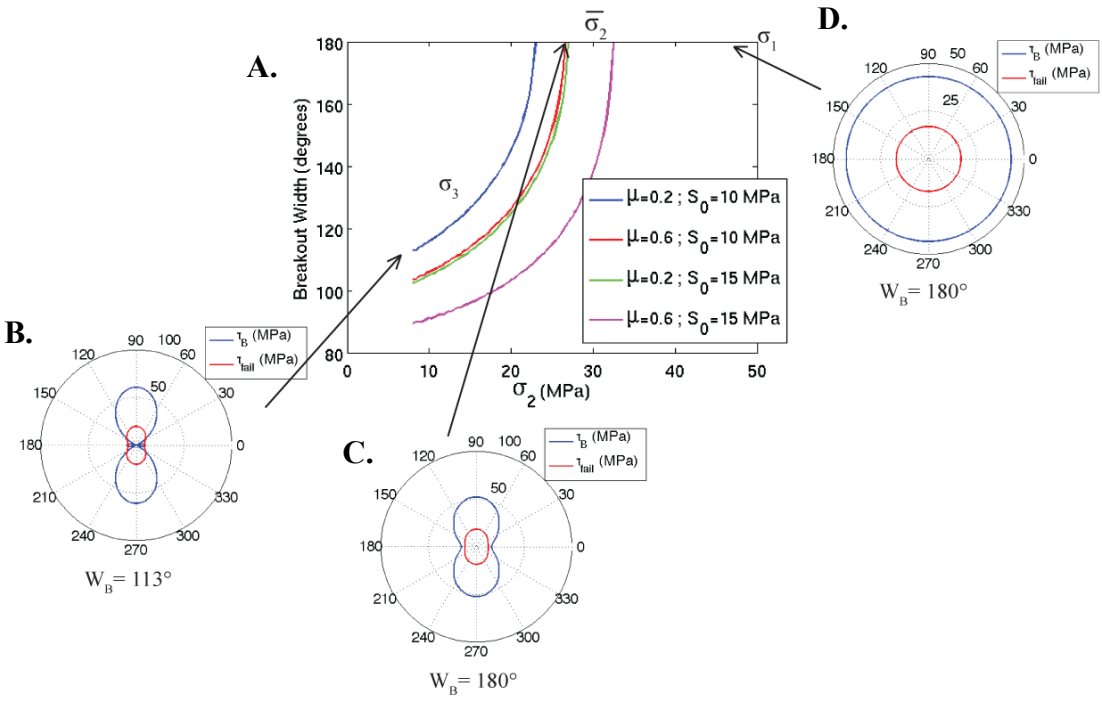

Figure 12. A. Breakout width as a function of the intermediate principle stress, σ_2, for the shallow-dip reverse fault at failure stress regime at 800 m sediment depth. Four cases are considered, by combining reasonably high and low values of the coefficient of friction, μ, and the cohesion, S_0, of the rock. Polar plots of the shear stress acting around the circumference of the borehole are shown for case 1 (μ = 0.2 and S_0 = 10 MPa) of shallow-dip fault at failure stress regime at: **B.** $\sigma_2 = \sigma_3$, **C.** $\sigma_2 = \bar{\sigma}_2$, and **D.** $\sigma_2 = \sigma_1$. Where the failure condition is reached ($\tau_B > \tau_{fail}$), the borehole will experience breakouts at that azimuth. The azimuth of S_{hmin} is 90° and 270°, whereas the azimuth of S_{Hmax} is at 0° and 180°.

Andersonian Normal Fault

In the Andersonian normal faulting regime, the borehole is expected to be stable for the proposed conditions of this drill site. Figure 13 A shows that this farfield stress regime results in a system that is completely stable at the planned borehole depth, 900 m below the sea floor. The failure condition ($\tau_B > \tau_{fail}$) is not reached for any value of σ_2 or combination of μ and S_0 studied. Figure 13 B-D shows breakout width (W_B) at σ_3, $\overline{\sigma}_2$ and σ_1 (respectively) on a horizontal cross-section of the vertical borehole for case 1, where $\mu = 0.2$ and $S_0 = 10$ MPa, as an example.

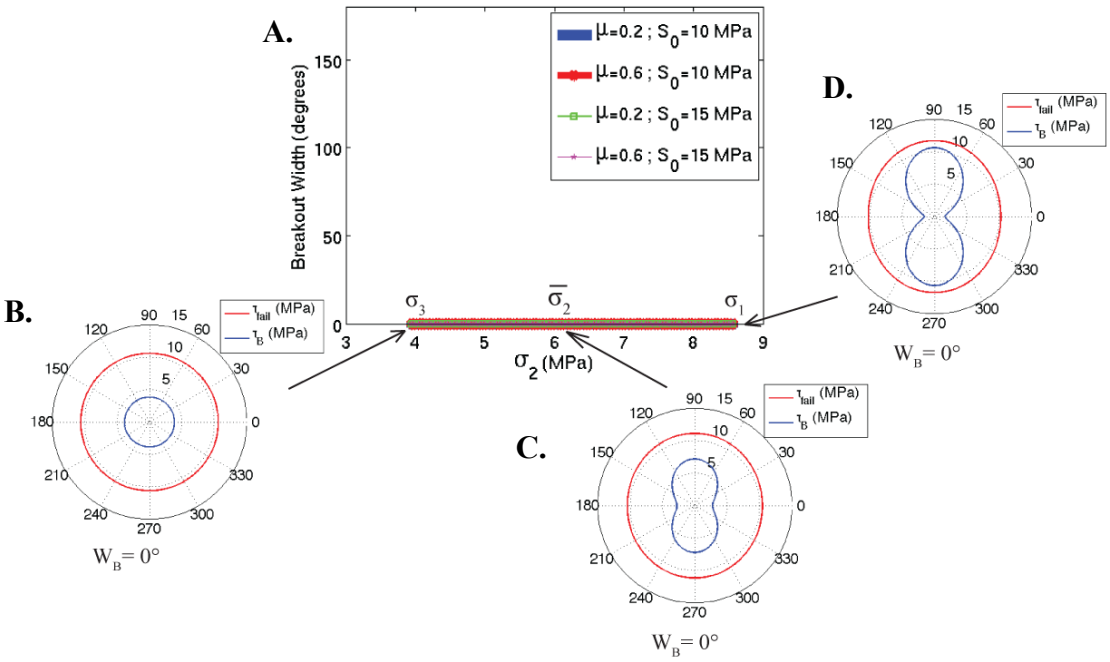

Figure 13. A Breakout width as a function of the intermediate principle stress, σ_2, for the Andersonian normal fault farfield stress regime at 900 m sediment depth. Four cases are considered, by combining reasonably high and low values of the coefficient of friction, μ, and the cohesion, S_0, of the

rock. Polar plots of the shear stress acting around the circumference of the borehole are shown for case 1 ($\mu = 0.2$ and $S_0 = 10$ MPa) of the Andersonian reverse fault stress regime at: **B.** $\sigma_2 = \sigma_3$, **C.** $\sigma_2 = \bar{\sigma}_2$, and **D.** $\sigma_2 = \sigma_1$. Where the failure condition is reached ($\tau_B > \tau_{fail}$), the borehole will experience breakouts at that azimuth. The azimuth of S_{hmin} is 90° and 270°, whereas the azimuth of S_{Hmax} is at 0° and 180°.

At the shallower depth of the target fault, 800 m into the sea floor, the borehole will experience lower stresses exerted around its perimeter than at the full depth, and will therefore not experience breakouts around at any azimuth around the borehole wall (Figure 14 A-D).

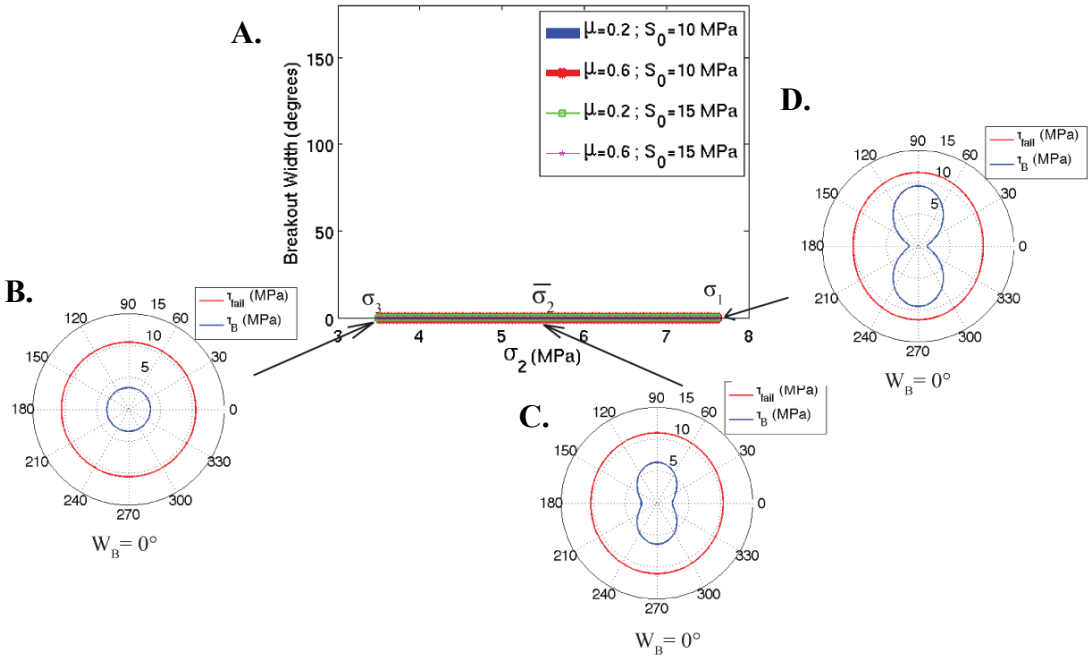

Figure 14. A Breakout width as a function of the intermediate principle stress, σ_2, for the Andersonian normal fault farfield stress regime at 800 m sediment depth. Four cases are considered, by combining reasonably high

and low values of the coefficient of friction, μ, and the cohesion, S_0, of the rock. Polar plots of the shear stress acting around the circumference of the borehole are shown for case 1 ($\mu = 0.2$ and $S_0 = 10$ MPa) of the Andersonian reverse fault stress regime at: **B.** $\sigma_2 = \sigma_3$, **C.** $\sigma_2 = \bar{\sigma}_2$, and **D.** $\sigma_2 = \sigma_1$. Where the failure condition is reached ($\tau_B > \tau_{fail}$), the borehole will experience breakouts at that azimuth. The azimuth of S_{hmin} is 90° and 270°, whereas the azimuth of S_{Hmax} is at 0° and 180°.

Discussion

Failure of the borehole depends strongly on the farfield stress state and rock strength. Both catastrophic failure and successful completion are possible for realistic scenarios. Results also show that stability of the borehole is sensitive to the drilling depth. In all three farfield stress regimes, the borehole will experience an increase in the magnitude of stresses exerted around the circumference with depth. This overall increase in stress can produce wider breakouts, and therefore exacerbate failure of the borehole wall. The Andersonian reverse fault stress regime is most affected by the increase in depth, as two of the rock strength cases (case 2, where $\mu = 0.6$ and $S_0 = 10$ MPa and case 3, where $\mu = 0.2$, $S_0 = 15$ MPa) evolved into a stress state that produced complete failure around the borehole wall as σ_2 increased, from 800 m to 900m depth below the sea floor.

The greatest range of stability variation is possible in the Andersonian reverse faulting regime. Case 1, with the low coefficient of friction value and lower of the two selected cohesion values ($\mu = 0.2$ and $S_0 = 10$ MPa), displays failure in the weakest rock conditions studied and is expected to cause catastrophic failure of the borehole. The relationship between rock strength and intermediate stress for cases 2 ($\mu = 0.6$ and $S_0 = 10$ MPa) and 3 ($\mu = 0.2$ and $S_0 = 15$ MPa) is not as clear. These cases represent a system

that is evolving toward a stable condition at 800 m depth, but further evolve towards complete failure as depth is increased to 900 m. As expected, when the rock strength is high ($\mu = 0.6$ and $S_0 = 15$ MPa), breakouts are not expected around the borehole circumference. At the shallower depth of the fault, both complete failure and a stable well are possible, but results indicate less failure (or more stability) than the full depth of the borehole. While this farfield stress model allowed us to calculate stress values using assumptions from the Andersonian classification scheme for a generic thrust environment, it may not accurately describe the stress regime of the Tohoku thrust fault system.

The shallow-dip fault at failure more closely approximates the orientation of the Tohoku fault zone, and therefore may be a more reasonable model for the farfield stress regime than the Andersonian reverse fault. In this model, however, the dip is near the horizontal plane of the borehole breakouts, at which complete failure is expected. Figures 11 and 12 confirm this result, as the calculations were made assuming that the farfield stresses were at the point of failure. The borehole will collapse in this farfield stress regime, even if depth is reduced to the target fault. If the fault experienced complete stress drop after March 11, 2011 it will not be critically stressed and this model will not be a valid approximation of the farfield stress regime of the Tohoku fault zone. Ide *et. al.* (2011) and Hasegawa *et. al.* (2011) have suggested that the fault experienced a complete, or near complete, stress drop from the Tohoku-Oki earthquake. If this is the case, then the shallow dip fault at failure end member is the least likely stress regime acting on the Tohoku fault currently. If JFAST is successful, and the borehole does not fail

catastrophically, this will be a good indication that there was a complete stress drop on the fault.

The Andersonian normal faulting model approximates farfield stress regime if the Tohoku fault zone evolved into an extensional system following complete stress drop on the fault. This may have occurred as a result of the anomalously large slip that occurred updip of the trench. If Ide *et. al.* (2011) and Hasegawa *et. al.* (2011) are correct in their studies suggesting that the Tohoku fault experienced complete stress drop following the March 11, 2011 event, then the normal faulting regime is a more likely prediction of stability on the borehole to be drilled in April and May 2012 during the JFAST operation. This stress model is not expected to produce failure of the proposed borehole for any combination of coefficient of friction or cohesion, across the entire range of the intermediate stress, even at the greater depth of 900 m below the ocean floor.

Zoback (2010) stated that 120° of total borehole failure ($W_B = 60°$) is a conservative value for the breakout width, as thousands of wells have been studied that do not experience significant failure at 60° breakouts, and the maximum breakout width that does compromise borehole stability is the empirically derived width of 90° in vertical wells. Results of this study indicate that, depending on farfield stress state, there may still be a high likelihood that the proposed borehole into the Tohoku fault zone will be unstable and experience breakouts widths much greater than 90°, leading to washouts and borehole collapse from the loss of arch-support in the well.

An important way to increase borehole stability according to Zoback (2010) is to raise the circulating mud weight (P_{mud}) used during drilling. This study assumed the mud weight to be equal to the pore pressure (i.e., no mud using during drilling). To fully

examine borehole stability, more research should be directed at the feasibility of using mud during drilling and at what densities, with corresponding corrections to be made to the calculations performed in this study.

When determining the density of mud to use during drilling, however, the chemical interactions between the mud and clay-rich rocks of the ocean floor must also be considered. These chemical interactions can affect local rock strength and pore pressure, and potentially exacerbate borehole failure (Zoback, 2010). Mud with a higher salinity than pore fluid can increase local pore pressure through osmosis and lead to borehole instability. The amount of ion exchange possible between the mud and pore fluid, as well as the replacement of cations (i.e. Mg^{2+} by Ca^{2+} and Na^{+} by K^{+}) can also weaken the formation, particularly in shales (Zoback, 2010). The density and composition of any mud used will need to be carefully analyzed to avoid the chemical effects, but still provide enough stability in the borehole to keep it from collapsing in on itself. With the addition of mud weight and mud chemistry, future studies will more accurately predict the expected failure conditions within the well and gain a better understanding of the stability of the proposed borehole to be drilled into the Tohoku fault zone during the JFAST cruise.

In the event that the boreholes are unstable and experience catastrophic failure, the Expedition 343 Scientific Prospectus outlines a contingency plan, subject to change depending on conditions during the expedition and by decision of the JFAST Project Management Team (Mori, *et. al.,* 2012). Due to the significant technical and logistical challenges for the expedition, particularly the potential for failure from the great

pressures at the total drilling depth as described above, four alternate sites have been identified (Figure 15).

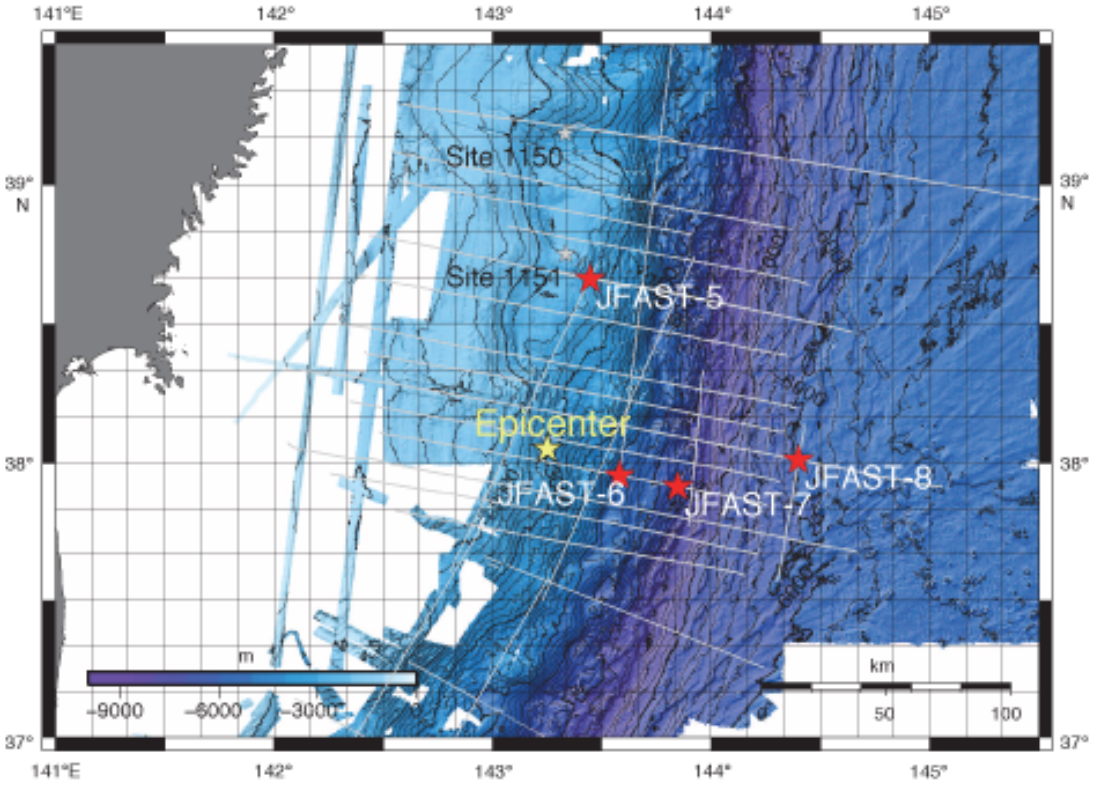

Figure 15. Possible contingency sites. From Mori, *et. al.,* 2012, p. 31.

Studies of the borehole breakouts experienced after drilling will be used to determine absolute stress levels. These absolute stress level estimates are important to study fault coupling along the Tohoku megathrust fault (Mori, *et. al.,* 2012). The importance of the JFAST project, and the many physical, chemical, and stress measurements planned to increase our understanding of fault mechanics and the processes that result in large subduction zone earthquakes, is without question. The

scientific community, and the general population as a whole, will benefit greatly for years to come from the knowledge obtained from the JFAST expedition.

Conclusion

This study used three possible farfield stress regimes to predict stability of a borehole to be drilled into the Tohoku fault zone, off the western coast of Honshu, Japan. Stability was tested over a range of coefficient of friction, cohesion, intermediate stress and drill depth values to arrive at more realistic and more robust conclusions. Table 2 lists the results of the stability analyses presented in this study by the potential farfield stress regime of the system.

Table 2: Results of stability analyses for the planned borehole by farfield stress regime, drill depth and rock strength.

	Depth below sea floor	Case 1: $\mu = 0.2$ $S_0 = 10$ MPa	Case 2: $\mu = 0.6$ $S_0 = 10$ MPa	Case 3: $\mu = 0.2$ $S_0 = 15$ MPa	Case 4: $\mu = 0.6$ $S_0 = 15$ MPa
Andersonian Reverse Fault	900 m total depth	Always Fails	Becomes more unstable with increasing σ_2, failure possible at large σ_2	Becomes more unstable with increasing σ_2, failure possible at large σ_2	Always Stable
	800 m to target fault	Always Fails	Becomes more stable with increasing σ_2, doesn't fail	Becomes more stable with increasing σ_2, doesn't fail	Always Stable
Shallow Dip Fault at Failure	900 m total depth	Always Fails	Always Fails	Always Fails	Always Fails
	800 m to target fault	Always Fails	Always Fails	Always Fails	Always Fails
Andersonian Normal Fault	900 m total depth	Always Stable	Always Stable	Always Stable	Always Stable
	800 m to target fault	Always Stable	Always Stable	Always Stable	Always Stable

Results indicate that an Andersonian reverse faulting farfield stress regime will be highly sensitive to variations in the value of the intermediate stress, the coefficient of friction and cohesion of the rock, and the depth of drilling below the sea floor. Stability on this end member ranges from catastrophic failure of the borehole ($W_B > 90°$) to a stable well ($W_B = 0°$), with increasing failure occurring with depth. The stress regime of a shallowly dipping fault at failure will produce catastrophic failure of the borehole ($W_B > 90°$) for all values tested. This stress regime represents a fault at failure, which is not likely the case following the M_w 9.0 event. The Andersonian normal faulting farfield stress regime does not produce failure of the borehole for any of the variations in values tested ($W_B = 0°$). This farfield stress regime is believed to have occurred as a result of complete stress drop and a change to extensional stress orientation on the fault. Results of this study give likely scenarios for borehole stability, depending on the current farfield stress regime. The Andersonian normal fault farfield stress regime would be most likely to approximate the actual farfield stress state of the Tohoku fault zone if it did experienced complete stress drop after the March 11, 2011 earthquake, whereas the farfield stress regime of the shallowly dipping fault at failure would be least likely.

References Cited

1. Anderson, E. M., 1951. *The dynamics of faulting and dyke formation with applications to Britain*. Edinburgh, Oliver and Boyd.

2. Brodsky, E. E., Ma, K.-F., Mori, J., Saffer, D. M., and the participants of the ICDP/SCEC International Workshop. "Rapid Response Fault Zone Drilling: Past, Present, and Future." *Scientific Drilling*, No. 8, September 2009. 66-74. doi:10.2204/iodp.sd.8.11.2009.

3. Hasegawa, A., Yoshida, K., and Okada, T. 2011. Nearly complete stress drop in the 2011 *M*w 9.0 off the Pacific coast of Tohoku Earthquake. *Earth Planets Space*, **63**, 703–707. doi:10.5047/eps.2011.06.007.

4. Hussong, D. M., Uyeda, S., et al., 1981. Deep Sea Drilling Project Leg 60: Cruise Objectives, Principal Results, and Explanatory Notes. Init. Repts. DSDP, 60: Washington (U.S. Govt. Printing Office). doi:10.2973/dsdp.proc.60.101.1982

5. Ide, S., Baltay, A., and Beroza, G. C., 2011. Shallow Dynamic Overshoot and Energetic Deep Rupture in the 2011 *M*w 9.0 Tohoku- Oki Earthquake. Science Express. 19 May 2011, 0.1126/science.1207020, < www.sciencexpress.org >

6. Marone, C., and Saffer, D. M. "Fault Friction and the Upper Transition from Seismic to Aseismic Faulting." *The Seismogenic Zone of Subduction Zone Thrust Faults*. Ed. Timothy H. Dixon and J. Casey Moore. Columbia University Press, New York, NY, 2007. 346-369. Print.

7. Moore, J. C., Rowe, C., and Meneghini, F. "How Accretionary Prisms Elucidate Seismogenesis in Subduction Zones." *The Seismogenic Zone of Subduction Zone Thrust Faults*. Ed. Timothy H. Dixon and J. Casey Moore. Columbia University

Press, New York, NY, 2007. 288-315. Print.

8. Mori, J., Chester, F. M., Eguchi, N., and Toczko, S. Integrated Ocean Drilling Program Expedition 343 Scientific Prospectus: Japan Trench Fast Earthquake Drilling Project (JFAST). Integrated Ocean Drilling Program Management International, Inc., for the Integrated Ocean Drilling Program, February 2012.
9. Mori, J., Kodaira, S., Brodsky, E. E., *et al.* Japan Trench Fast Earthquake Drilling Project (J-FAST). IODP Proposal. July 2011.
10. Zoback, M. D. Reservoir Geomechanics. Cambridge University Press, New York, NY. 2010.